Chinese Journal of Chemical Engineering 94 (2026) 291–300

Contents lists available at ScienceDirect

Chinese Journal of Chemical Engineering

journal homepage: www.elsevier.com/locate/CJChE

Full Length Article

Extrusion of honeycomb monoliths of ZSM-5: A systematic method for determining the plasticity of zeolite pastes and optimizing extrusion workability

Zihao Zhou [1], Yingshu Liu [1, 2, *], Ningqi Sun [2, 3], Ziyi Li [1, *]

[1] School of Energy and Environmental Engineering, University of Science and Technology Beijing, Beijing 100083, China
[2] Songshan Lake Materials Laboratory, Dongguan 523808, China
[3] Institute of Physics, Chinese Academy of Sciences, Beijing 100190, China

ARTICLE INFO

Article history:
Received 1 September 2025
Received in revised form
26 December 2025
Accepted 29 December 2025
Available online 13 February 2026

Keywords:
Paste plasticity
Extrusion
Honeycomb monolith
Zeolite

ABSTRACT

Honeycomb monoliths of zeolites (HMZs) exhibit low pressure drop and high mass transfer efficiency due to their designable through-channels and the uniform distribution of the active phase throughout the structure which HMZs are promising for gas adsorption and separation applications under high space velocities and abrasive environments. However, most zeolites cannot be directly extruded due to their lack of plasticity similar to clay. Therefore, the plasticity of zeolite pastes needs to be determined for optimizing the extrusion process with an optimal composition. Here in, a novel analytical method was developed to characterize the plastic behavior of zeolite pastes based on the stress–deformation curve. This curve was divided into elastic, yield, and plastic zones under defined conditions. Empirical equations were also established to predict the extrusion workability of ZSM-5 zeolite pastes by considering the effects of their composition and preparation processes. The plastic behavior of the ZSM-5 zeolite paste differed from those of ceramic and clay pastes (such as Al_2O_3 and SiO_2), particularly in the plastic zone. Using montmorillonite as an inorganic binder prevented the formation of shear-thickening branches within the elastic zone of the stress–deformation curves, contrary to those observed in the curves for kaolin and attapulgite. Methyl cellulose and hydroxypropyl methyl cellulose enhanced the plasticity of the paste, and the latter improved the yield stress more effectively. The ZSM-5 zeolite paste, with a liquid–solid ratio of 44.5, successfully met the plastic-zone conditions without the influence of deformation rates and exhibited optimized extrusion workability. In addition, vacuum refining considerably enhanced extrusion workability by reducing the air content and interparticle spacing in the ZSM-5 powder. The accuracy of the proposed method for predicting the extrusion behavior of HMZs was verified *via* extrusion experiments. The results yielded valuable insights into optimizing the extrusion workability of zeolite pastes.
© 2026 The Chemical Industry and Engineering Society of China, and Chemical Industry Press Co., Ltd. All rights are reserved, including those for text and data mining, AI training, and similar technologies.

1. Introduction

Zeolites are crystalline aluminosilicates characterized by their high surface area and hydrothermal stability. Consequently, they are extensively used as catalysts and adsorbents in a variety of industrial contexts, including petrochemicals and coal chemicals as well as in various gas adsorption and separation processes [1,2]. The International Zeolite Association has recognized more than 250 zeolite frameworks and assigned a special three-letter code to each framework [3]. ZSM-5, which contains a high Si/Al ratio, is a commercial zeolite with an MFI structure [4]. Its powder form is typically synthesized *via* hydrothermal reactions. However, zeolite powders are not suitable for direct use due to their propensity for catalyst loss and their high resistance to gas flow [5]. Honeycomb monoliths with parallel channels have been shown to mitigate these issues by minimizing pressure drops under high gas flow rates and enhancing the utilization efficiency of zeolites [6,7]. Extrusion is regarded as an optimal method for manufacturing high-quality zeolite monoliths because it offers low production costs, high production efficiency, and shape and size flexibility.

* Corresponding authors.
E-mail addresses: liuyingshu@sslab.org.cn (Y. Liu), ziyili@ustb.edu.cn (Z. Li).

https://doi.org/10.1016/j.cjche.2025.12.037
1004-9541/© 2026 The Chemical Industry and Engineering Society of China, and Chemical Industry Press Co., Ltd. All rights are reserved, including those for text and data mining, AI training, and similar technologies.

Honeycomb monoliths of zeolites (HMZs) are extruded *via* four stages: paste preparation (wet mixing, kneading, aging, and vacuum refining); extrusion (extruding the paste from the die to obtain a honeycomb green body under pressure); drying; and calcination [8]. The plastic behavior of the zeolite paste primarily governs the extrusion of monoliths. Its plasticity is influenced by its composition, particle size, moisture content, processing method, temperature, and duration [9,10]. Unlike clay, most zeolites exhibit low plasticity and are not readily extrudable through the use of water alone. Although binder-free zeolite extrusions have been reported [11], zeolite–binder systems are irreplaceable because binders improve the workability of zeolite paste and enhance the mechanical strength of the extrudate. And the determination of the plasticity of zeolite paste is challenging because it cannot be directly applied and explained to the extrusion. Moreover, the methods available for the assessment of zeolite paste plasticity are limited and extrusion parameters are not adequately defined due to commercial confidentiality.

The plasticity of clay pastes is currently determined using Atterberg and Pfefferkorn plasticity index, stress–strain curves, and rheological measurements [12], whereas that of zeolite pastes has been scarcely reported. In particular, porous zeolites possess the capacity to absorb substantial quantities of liquids, such as added water, in contrast to clay plates. These liquids can be released from zeolites under compression and due to temperature variations, leading to instability in zeolite paste plasticity. Zeolite pastes are being extensively studied because the interactions among paste components are unclear; the impacts of various preparation processes on the extrudate quality are overlooked; and plasticity is determined only before extrusion. Li *et al.* [13] characterized 5A zeolite pastes by assessing the relationship between pressure drop and extrusion velocity during its flow from a circular barrel into a circular die land. Aranzabal *et al.* [8] reported that the H-ZSM-5 zeolite paste achieved the best rheological properties when wet kneading was stabilized at a drive torque of ~10 Nm. However, it is not straightforward to identify the key factors influencing the extrusion workability of zeolite pastes based on existing research. It is evident that the extrusion conditions of zeolite pastes can be elucidated *via* the compression testing by determining the modulus of elasticity, yield strength, maximum deformation, and rupture strength from the derived stress–deformation curves [14]. In the present study, the compressive deformation behaviors of zeolite pastes determined from stress–deformation curves facilitate the development of empirical formulas for extrusion workability. Furthermore, it is possible to establish a correlation between the plasticity of zeolite paste and the extrusion process by controlling the pastes composition and preparation methods.

In this study, an analytical method for evaluating the extrusion workability of zeolite pastes was proposed by analyzing the stress–deformation curve. The plastic behavior of the ZSM-5 zeolite paste was compared with those of zeolite-free pastes to determine its distinctive properties. The effects of binders, liquid–solid ratio, addition of emulsifiers, and preparation processes on the plasticity of the ZSM-5 zeolite paste were analyzed. Then, the accuracy of the proposed method was validated by extruding an optimized ZSM-5 zeolite paste.

2. Experimental

2.1. Materials

Commercial ZSM-5 (Zhuoran Environmental Protection Co., Ltd., Dalian, China) with a Si/Al ratio of 170 was used as the target zeolite. Industrial alumina powder (Branch Constant Crystal Material Co., Ltd., Zibo, China) containing >99.9% (mass) of Al_2O_3, and silica powder (Brofos Nanotechnology Co., Ltd., Kunshan, China) containing >99.99% (mass) of SiO_2 were used. Common commercial clays, including kaolin (China Kaolin Clay., Ltd., Suzhou, China), attapulgite (Jiangsu Huayuan MINING Co., Ltd., Huaian, China), and montmorillonite (Shandong Huawei Bentonite Co., Ltd, Weifang, China), were used as inorganic binders. Methyl cellulose, ethyl cellulose, and hydroxypropyl methyl cellulose (all purchased from Sinopharm Chemical Reagent Co., Ltd., Shanghai, China) were used as organic binders. LAE-9 (Wuhan Shuou Technology Co., Ltd., Wuhan, China) and deionized water were employed as an emulsifier and a plasticizer, respectively.

2.2. Preparation of HMZ

An HMZ monolith with a cross-sectional area of ~250 mm^2 was fabricated using ZSM-5 and clay as the primary raw materials *via* a process involving paste preparation, extrusion, drying, and calcination. Fig. 1 shows these procedures and typical sample images.

2.2.1. Preparation of paste

ZSM-5, inorganic binder, and organic binder were dry-mixed in a ball mill for ~20 min at 250 $r \cdot min^{-1}$, with a mass ratio of raw

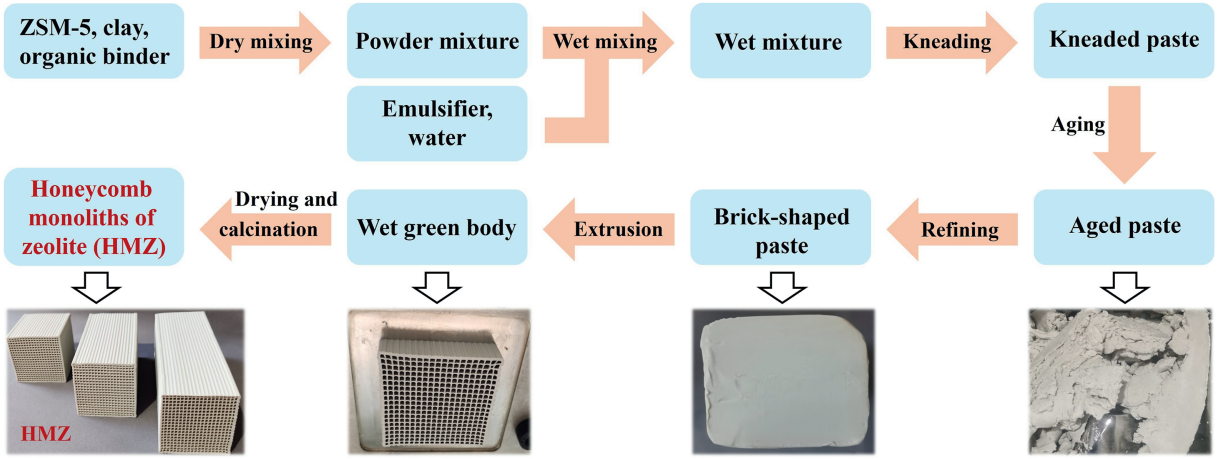


Fig. 1. Preparation procedures of HMZ and typical sample images.

materials to grinding ball = 1:4. Then, the emulsifier and deionized water were added into the mixture, which was subjected to 15 min of wet mixing. Tables S1–S3 (in Supplementary Material) show the paste composition. The wet-mixed paste was kneaded for 10 min and sealed and aged at room temperature for more than 24 h. The aged paste was subjected to vacuum refining for 20 min in a JN30/25 de-airing extrusion unit (Hunan Zhonglian Ceramic Machinery Co., Ltd, Hunan, China), and the brick-shaped sample was subsequently extruded.

2.2.2. Extrusion, drying, and calcination

The brick-shaped sample was extruded into a wet green body with a square-hole honeycomb pattern using a horizontal vacuum extruder. Three dies with different pore sizes were self-designed (Table S4) and classified into die-90, die-60, and die-15 based on the cell density (cell per in^2). The extrusion rate was determined by using a contact meter. Dry green body with a moisture content below 0.1% produced *via* microwave drying. The HMZ was fabricated *via* calcination in a muffle furnace under air, with a heating rate of 2 °C·min^{-1} and the final temperature maintained for over 2 h.

2.3. Characterization of HMZs

The density of the paste was measured using an FMS-120 mud density meter (Suzhou Danster Electronics co., Ltd, Shanghai, China) according to the standard JJG 1045-2017 (China). Powder X-ray diffraction (XRD) patterns were measured using a X'Pert Pro diffractometer (PANalytical, Netherlands) with nickel-filtered Cu K_α radiation at a scanning rate of 2.0 (°)·min^{-1} and scanning angles of 5°–50°. Scanning electron microscopy (SEM) images were captured on a XL30 electron microscope (Philips, Netherlands) operating at 20 kV. A TG 209 F3 Farsus thermogravimetric analyzer (Netzsch, Germany) was used to perform thermogravimetric analysis (TGA) in an air atmosphere, with a heating rate of 10 °C·min^{-1}. Mass variations were determined using DSC 214 Polyma differential scanning calorimeter (Netzsch, Germany) in an air atmosphere and at a heating rate of 10 °C·min^{-1}. Argon sorption isotherms were measured at 87 K using an ASAP 2020 analyzer (Micrometrics, USA). The specific surface area (SSA) was determined by the Brunner–Emmet–-Teller (BET) method using the relative pressure (P/P_0) in the range of 0.05–0.3. The pore size distribution (PSD) of micropores and mesopores were calculated by Horvath–Kawazoe (HK) and Barrett–Joyner–Halenda (BJH) methods, respectively. The pore volume was derived from the maximum adsorption capacity at a relative pressure (P/P_0) of 0.99. The micropore volume and micropore surface area (internal surface area) were calculated using the *t*-plot method. Uniaxial compression tests were performed to investigate the plastic behavior of zeolite pastes based on the findings reported by Baran *et al.* [15], Tajiri *et al.* [16] and Al-Qureshi *et al.* [17] for plasticity clays. The plasticity was tested using the PT-305B mechanical testing device (Dongguan Quality Control Instrument Co., Ltd., Dongguan, China), equipped with a 0–500 N pressure sensor and operated at a compression rate of 5–45 mm·min^{-1}.

3. Results and Discussion

3.1. Extrusion workability of zeolite pastes

The composition of raw materials and preparation processes considerably impacted the extrusion of brick-shaped zeolite samples. Fig. 2 shows the stress–deformation curve of a zeolite paste with good extrusion workability. The analysis of the plastic

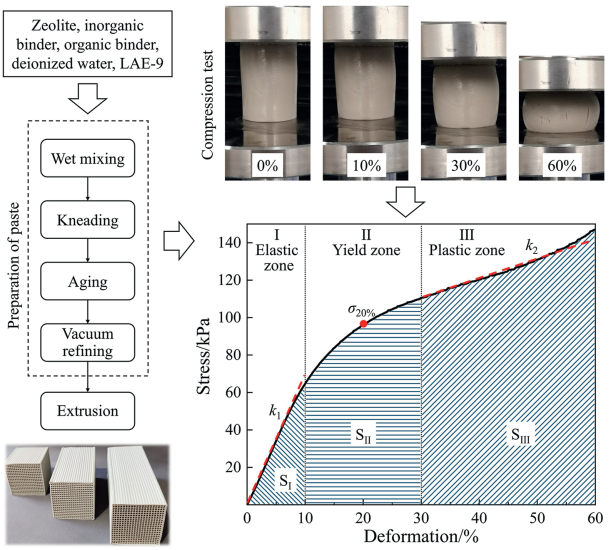


Fig. 2. Determination and analysis of the stress–deformation curve of zeolite pastes.

deformation behaviors of zeolite pastes based on compressive stress–deformation curves for metallic materials [15–18], ceramic pastes [19] and clays [20]. And the elastic zone (1% to 10%), yield zone (10% to 30%), and plastic zone (30% to 60%) are defined based on the stress–deformation curves derived for over 50 ZSM-5 paste compositions. An extruded zeolite paste generally satisfies the following conditions, provided that if its volume remains unchanged during compression:

(I) Elastic zone

The fitting curve must conform to the first-order equation, with $R^2 > 0.99$ (goodness of fit).

$$\sigma = k_1 \varepsilon \tag{1}$$

where σ denotes the stress, kPa; k_1 is the slope of the fitted curve within the elastic zone; and ε is the deformation, %.

(II) Yield zone

The stress value at 20% deformation is defined as yield stress.

$$\sigma_{\text{yield}} = \sigma_{20\%} \tag{2}$$

where σ_{yield} is the yield stress, kPa; and $\sigma_{20\%}$ is the stress at 20% deformation, kPa.

(III) Plastic zone

The fitting curve should conform to the first-order equation, with $R^2 > 0.98$.

$$\sigma = k_2 \varepsilon + b \tag{3}$$

where σ is the stress, kPa; k_2 is the slope of the fitted curve within the plastic zone; ε is deformation, %; and b is the intercept of the fitting curve.

The plastic deformation behavior of zeolite paste is difficult to attribute to plastic zone control, owing to the absence of significant work hardening and the dynamic recrystallization processes

comparable to metallic materials [21,22]. Moreover, the elastic zone and yield stress also influence the curve distribution of the plastic zone. To directly determine the extrusion workability of zeolite pastes, the empirical equations for the composition and preparation process of the clay material were proposed for the first time (satisfying the elastic zone and plastic zone conditions).

The extrusion workability of paste with identical preparation processes is significantly correlated with yield strength and the plasticity zone. And the extrusion workability of pastes with varying compositions is the product of their yield stress and the area of the plastic zone.

$$E_w = \sigma_{20\%} \int_{0.3}^{0.6} (k_2\varepsilon + b)\mathrm{d}\varepsilon \tag{4}$$

where E_w is the extrusion workability.

Suitable preparation processes can effectively enhance the plasticity of the paste. Moreover, its plastic behavior is related to the proportion of the plastic zone area. The extrusion workability of pastes with the same composition and different preparation processes was determined as follows:

$$E_w = \int_{0.3}^{0.6} (k_2\varepsilon + b)\mathrm{d}\varepsilon \Big/ \left(k_2 \int_{0}^{0.6} \sigma \mathrm{d}\varepsilon \right) \times 100\% \tag{5}$$

3.2. Distinctive properties of zeolite pastes

The stress–deformation curves of the ZSM-5 paste and zeolite-free pastes were compared to determine the characteristics of the former. As ZSM-5 has high porosity and water absorption capacity, the liquid–solid ratio of the ZSM-5 paste was considerably higher than those of zeolite-free pastes. Although the added water reduced the deformation resistance of the ZSM-5 paste, its yield strength remained high (Fig. 3). In the plastic zone (30% to 60% deformation), the stress–deformation curve for the ZSM-5 paste exhibited a linear increase. In contrast, the curves for alumina and silica pastes showed uniform plastic deformation, whereas that for montmorillonite paste showed a downward trend due to cracking. This indicated that the ZSM-5 paste exhibited different deformation behavior than those of ceramic and clay pastes, and its stress–deformation curve showed distinct zones and a continuous upward trend.

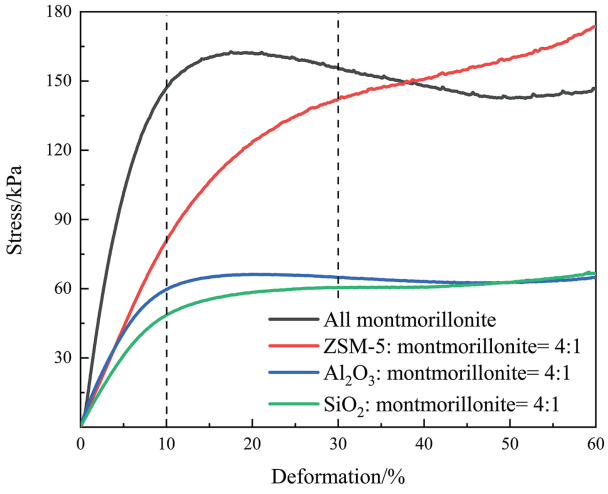


Fig. 3. Stress–deformation curves of the ZSM-5 paste and zeolite-free pastes.

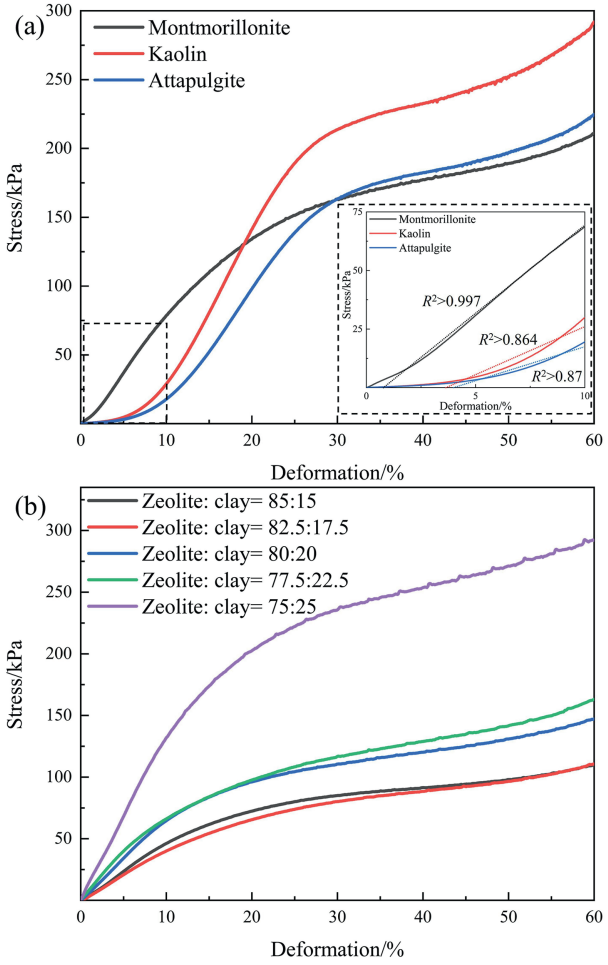


Fig. 4. Stress–deformation curves for ZSM-5 pastes containing different inorganic binders: (a) types of inorganic binders and (b) contents of montmorillonite.

3.3. Optimization of extrusion workability of zeolite pastes

3.3.1. Effect of inorganic binders

Fig. 4(a) shows the stress–deformation curves of ZSM-5 pastes containing different inorganic binders (deformation rate = 5 mm·min^{-1}). The inorganic binder mass content (13.1%), particle size (D_{50} = 5 μm), and preparation processes of the three pastes were kept consistent. The stress–deformation curve for the ZSM-5 paste containing kaolin or attapulgite as an inorganic binder exhibited pronounced shear-thickening branches [18] and the goodness of fit well below 0.99 in the 0% to 10% deformation range. However, that for the ZSM-5 paste containing montmorillonite perfectly conformed to the linear equation with $R^2 > 0.997$. For extrusion, ZSM-5 pastes must exhibit stable plastic behavior, particularly avoiding shear thinning and thickening. Montmorillonite particles rearrange and are bound by capillary forces during deformation of the corresponding ZSM-5 paste, rendering montmorillonite suitable for extrusion. This inorganic binder mainly influenced the elastic zone of the stress–deformation curve.

Fig. 4(b) shows the stress–deformation curves for ZSM-5 pastes with different mass contents of montmorillonite (compression rate = 5 mm·min^{-1}) and 30.0% of water. All the curves exhibited the characteristic elastic, yield, and plastic zones. The stress steadily increased with increasing montmorillonite content for the same deformation, showing a notable increment at a ZSM-5: montmorillonite ratio of 75:25. When the montmorillonite mass

content exceeded 25% (relative to ZSM-5), an excess amount of water was required for preparing the ZSM-5 paste. The liquid between particles generally acts as a plasticizer [23]. However, as ZSM-5 and montmorillonite have different water absorption capacities, the ZSM-5 paste containing a high montmorillonite content lacked sufficient liquid water film to reduce particle friction. These findings indicate that the plasticity of ZSM-5 pastes can be considerably improved by adding appropriate amounts of montmorillonite and water. Therefore, a ZSM-5:montmorillonite ratio of 80:20 was used for subsequent experiments to ensure an adequate ZSM-5 content in the monolith and excellent extrusion workability.

3.3.2. Effect of organic binders

Generally, binders also enhanced the plasticity, hardness and cohesion of zeolite pastes. And the cellulose was defined as an organic binder to distinguish it from inorganic binders. However, the effect of a single binder on pastes was limited. Two or more binders were often mixed to make pastes suitable for extrusion. Moreover, the binder content was also controlled by the state of the pastes. For example, the extrusion workability of ZSM-5 paste containing 10% (mass) HPMC was extremely poor (Fig. S2). Because the sample sustained severe cracking during compressive deformation.

Three commercially available cellulose types with similar viscosities were used as organic binders (2.4% (mass)) in ZSM-5 pastes. Fig. 5(a) shows their corresponding stress–deformation curves (compression rate = 5 mm·min^{-1}). The stress–deformation curves for the ZSM-5 paste containing ethyl cellulose (EC) and that without organic binders were similar, showing pronounced shear-thickening branches ($R^2 < 0.98$) at 30% to 60% deformation; this indicated that EC primarily enhanced the strength of ZSM-5 pastes rather than their plasticity. In contrast, the curves for ZSM-5 pasts containing methyl cellulose (MC) and hydroxypropyl methyl cellulose (HPMC) conformed to the first-order equation with $R^2 > 0.98$. The higher stress values observed for the HPMC-containing ZSM-5 paste indicated that both HPMC and MC could improve the plasticity of ZSM-5 pastes, with the former more effectively enhancing the extrusion workability. These findings also confirmed that organic binders mainly affected the plastic zone of the stress–deformation curve.

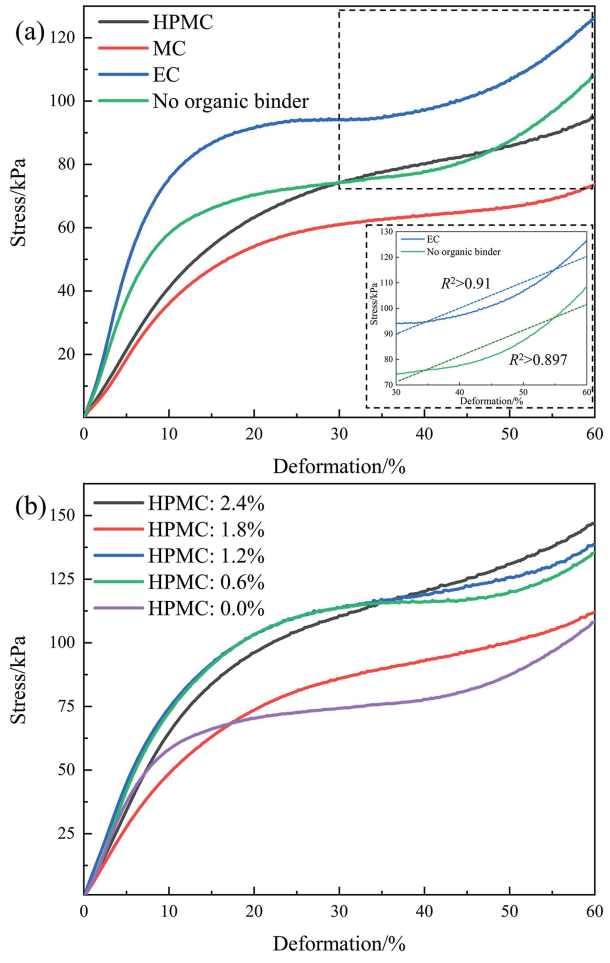


Fig. 5. Stress–deformation curves for ZSM-5 pastes containing different organic binders: (a) types of organic binders and (b) mass contents of HPMC.

The influence of HPMC content on the plasticity of the ZSM-5 paste was investigated to clarify its influence mechanism. Fig. 5(b) shows the stress–deformation curves of ZSM-5 pastes containing different HPMC contents (compression rate = 5 mm·min^{-1}). The curves showed pronounced shear-thickening branches at 30% to 60% deformation until the HPMC mass content decreased to 0.6%. Interestingly, the ZSM-5 paste containing 1.8% of HPMC exhibited the lowest yield stress ($\sigma_{20\%}$) among all samples (excluding that containing 0.0% of HPMC), suggesting that the plasticity of ZSM-5 pastes can be improved further using an optimal HPMC content. ZSM-5 pastes containing more than 1.2% of HPMC exhibited higher yield stress and achieved extrusion workability in the plastic zone almost similar to that of the ZSM-5 paste containing 2.5% of HPMC. These findings indicate that the plasticity and extrusion workability of the ZSM-5 paste can be effectively improved using an HPMC content of 1.2%.

3.3.3. Effects of liquid–solid ratio and LEA-9 contents

Based on optimal montmorillonite and HPMC contents, the effect of liquid–solid ratio and LEA-9 content on the plastic behavior of ZSM-5 paste was analyzed. The yield stress and deformation without rupture were simultaneously controlled by adjusting the water content in the ZSM-5 paste. Fig. 6(a) shows the stress–deformation curves for ZSM-5 pastes with different liquid–solid ratios (compression rate = 5 mm·min^{-1}). The yield stress continuously decreased with increasing liquid–solid ratio, with an optimal extrusion workability. The stress–deformation curve for the ZSM-5 paste with a liquid–solid ratio of 41.4 showed a high yield stress (about twice that of the ZSM-5 paste with a liquid–solid ratio of 44.5) and small shear-thickening branches, indicating that their extrusion workability was easily influenced by water content before reaching the critical state. For instance, the extrusion workability of the ZSM-5 paste with a liquid–solid ratio of 47.6 only reduced by ~18% compared with that of the ZSM-5 paste with a liquid–solid ratio of 44.5. The effect of LEA-9 on the ZSM-5 paste was similar to that of added water (Fig. 6(b)). The yield stress of ZSM-5 pastes decreased with increasing LAE-9 content, and their extrusion workability effectively improved only when the LAE-9 mass content exceeded 3.2%. This indicated that emulsifiers effectively reduced the resistance between zeolite and clay particles.

3.3.4. Optimization of liquid–solid ratio of ZSM-5 pastes

The extrusion workability of ZSM-5 pastes with different liquid–solid ratios was determined at different deformation rates. Fig. 7 shows the corresponding results, wherein almost all ZSM-5 pastes (except that with a liquid–solid ratio of 41.4) meet the plastic-zone conditions ($R^2 > 0.98$) at a deformation rate of 5 mm·min^{-1}. However, the differences in their plasticity gradually

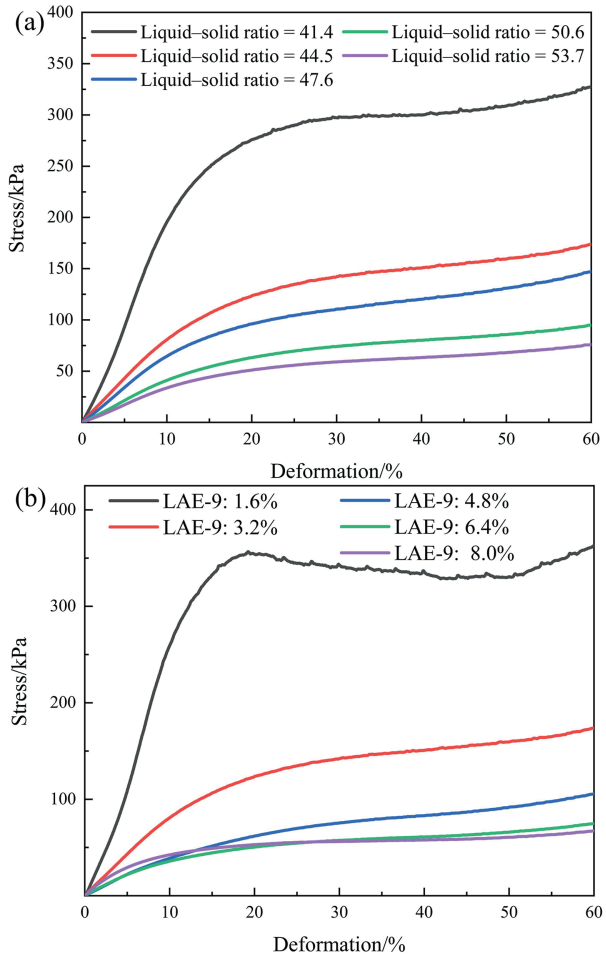


Fig. 6. Stress–deformation curves for ZSM-5 pastes with different liquid phase content: (a) liquid–solid ratio and (b) mass content of LEA-9.

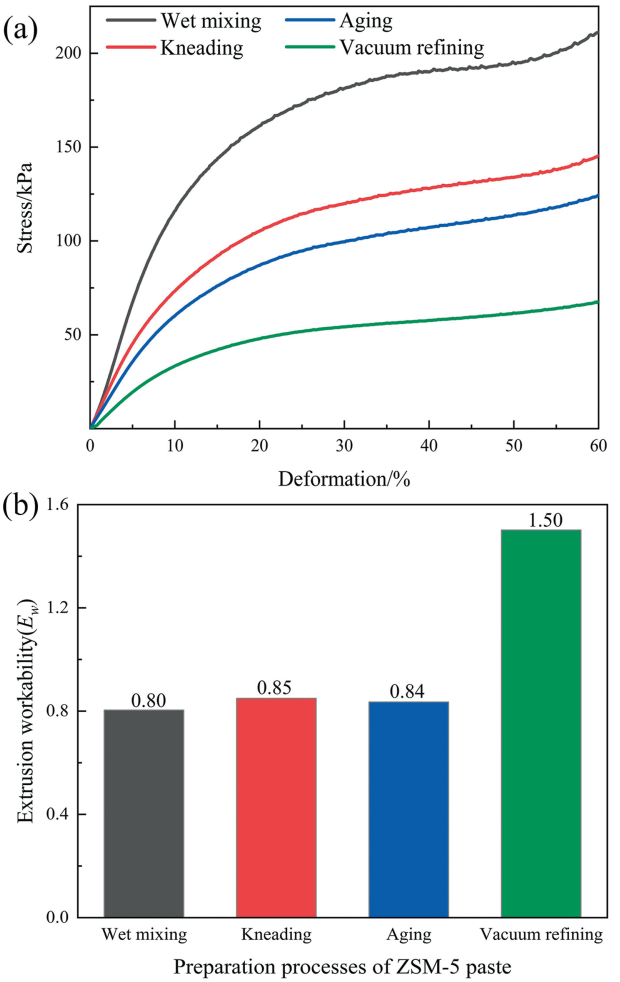


Fig. 8. (a) Stress–deformation curves of ZSM-5 paste prepared by different preparation processes. (b) Extrusion workability of ZSM-5 paste corresponding to the preparation processes.

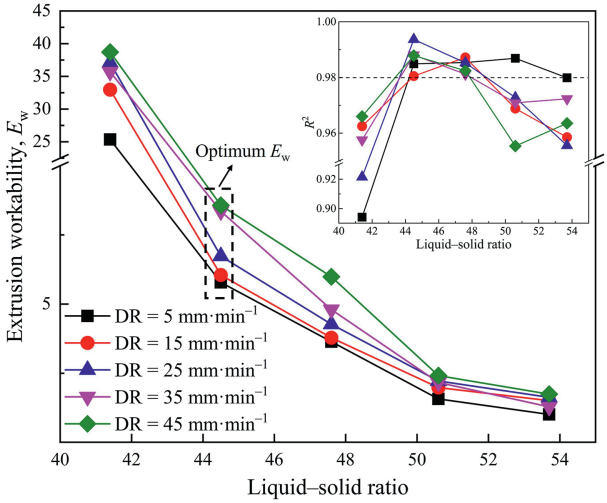


Fig. 7. Extrusion workability of ZSM-5 pastes with different liquid–solid ratios at different deformation rates (DR: deformation rate).

became obvious as the deformation rate increased, which can be attributed to the increasing yield stress. This indicated that the plastic behaviors of ZSM-5 pastes were influenced by deformation or extrusion rates. Zeolite pastes with low sensitivity to variations in the deformation rate are suitable for extrusion. Herein, only the pastes with liquid–solid ratios of 44.5 and 47.6 met the plastic-zone conditions (according to Eq. (4)) without being influenced by deformation rates, and that with a liquid–solid ratio of 44.5 exhibited better extrusion workability.

3.3.5. *Effect of preparation process*

Zeolite pastes are typically prepared *via* wet mixing, kneading, aging, and vacuum refining, and their plasticity is primarily determined by the final state of the pastes rather than the preparation processes. Fig. 8(a) shows the stress–deformation curve for ZSM-5 pastes prepared using different methods (compression rate = 5 mm·min^{-1}). The yield stress of the ZSM-5 paste prepared *via* vacuum refining was only one-fourth of that prepared *via* wet mixing. And the densities of ZSM-5 pastes gradually increased with the preparation processes (wet mixing, kneading, aging, and

vacuum refining), which were 1.493, 1.520, 1.518 and 1.541 g·cm^{-3}, respectively (Table S5). Interestingly, the extrusion workability of vacuum refined ZSM-5 paste (Fig. 8(b)) considerably improved according to Eq. (5) due to the continuous expulsion of air and reduction of interparticle spacing caused by repeated compressive force and evacuation.

3.4. Verification of the extrusion workability of the optimized ZSM-5 paste

The extrusion workability of zeolite paste is the macroscopic performance of its plasticity, rheology and hardness. Changing any single raw material within the zeolite paste will exert an irreversible effect upon its plastic behavior. For instance, zeolite paste only exhibits favorable extrusion workability when the liquid–solid ratio reaches a critical value. And the optimized preparation processes only partially improve the extrusion workability of the paste. However, the paste should possess sufficient plasticity to achieve good workability on its own. For example, vacuum refining enhances the extrusion workability of optimized paste.

The monolith quality is influenced by the optimal combination of pastes rheology, extrusion die specifications, and extruder motor power. The relationship between the flow rate of ZSM-5 pastes and extruder motor power was investigated using extrusion dies with various pore sizes. Fig. 9 shows that the flow rate of the ZSM-5 paste exhibits a linear relationship with the motor power, regardless of the type of extrusion dies. This indicated that the ZSM-5 paste can match various dies and extrusion rates due to its excellent extrusion workability. At a constant flow rate, a high motor power corresponds to a high forming resistance from the extrusion die. To minimize variations in the properties of extrudates resulting from differences in die specifications, ZSM-5 pastes were extruded at a flow rate of 5–6 cm^3·s^{-1}. And the mass of wet green bodies (the length was approximately 150 mm) formed by die-90, die-60 and die-15 were 245 ± 5 g, 297 ± 5 g and 274 ± 5 g respectively.

Due to the complexity of raw materials and preparation processes, most HMZs were obtained through repeated trial and error. The stability of the paste formulation and extrusion conditions were difficult to ascertain. In contrast, a mechanism for the influence of composition and preparation process on the extrusion workability of pastes had been established in this paper based on empirical formulas. And HMZs were prepared smoothly and stably using the optimal formulation.

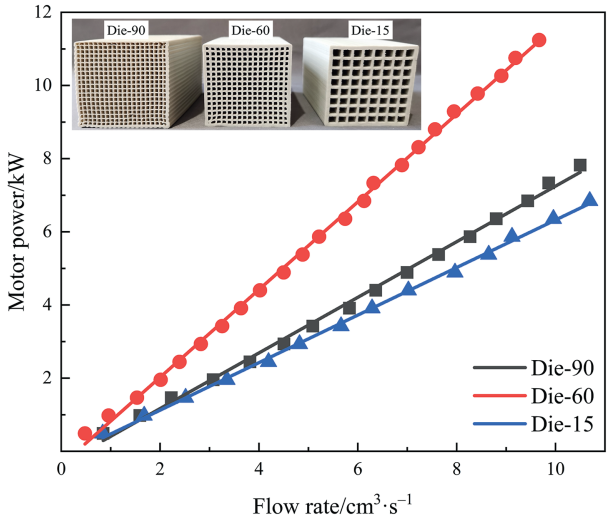


Fig. 9. Effects of die specifications on the flow rate of ZSM-5 paste and motor power.

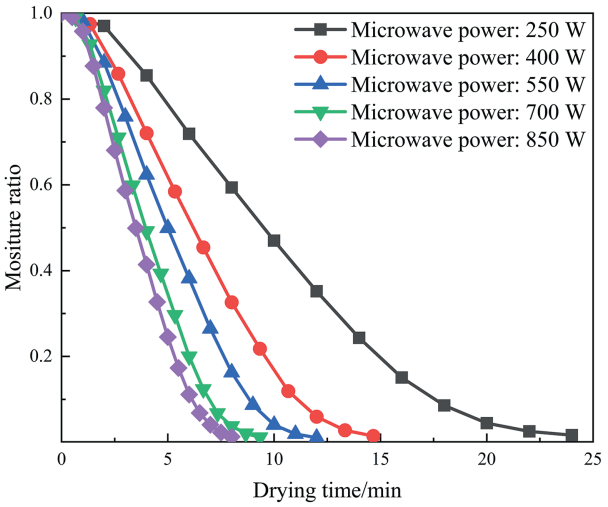


Fig. 10. Microwave drying curves of HMZs (drying a single HMZ with the same quality at each level of microwave power).

3.5. Drying and calcination of HMZs

The drying process of zeolite extrudates is more complex compared with that of ceramic extrudates. Due to the porous structure of zeolites and the difference in the drying shrinkage rates of zeolites and clay, the HMZ cracked and underwent nonuniform shrinkage. Microwave drying preserved the shape and structural integrity of fresh HMZ more effectively compared with oven drying [24]. Fig. 10 shows the microwave drying curve of the HMZ, indicating that microwave drying considerably reduced the drying time of the HMZ. The penetrability of microwaves, coupled with the strong absorption of microwave energy by moisture within the HMZ, enhanced the uniformity of drying and reduced the likelihood of cracking. The rate of moisture ratio reduction in the monolith was directly proportional to the microwave power.

Fig. 11 shows that the mass loss of dry HMZs without calcination continuously decreases within the temperature range of 30 °C–600 °C. Three distinct mass loss regions for dry HMZs were observed, attributed to the removal of adsorbed and interlayer

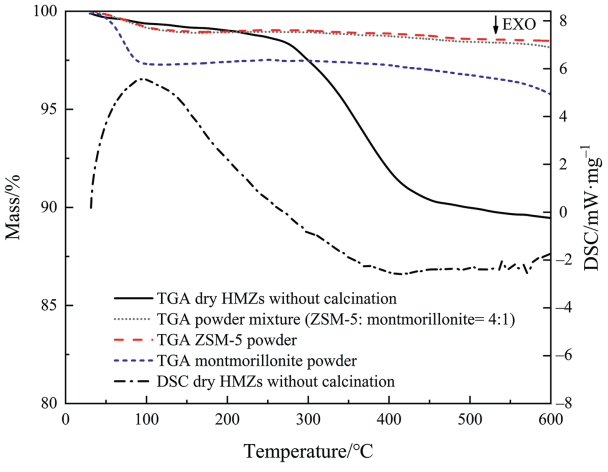


Fig. 11. TGA and DSC curves of raw materials and samples.

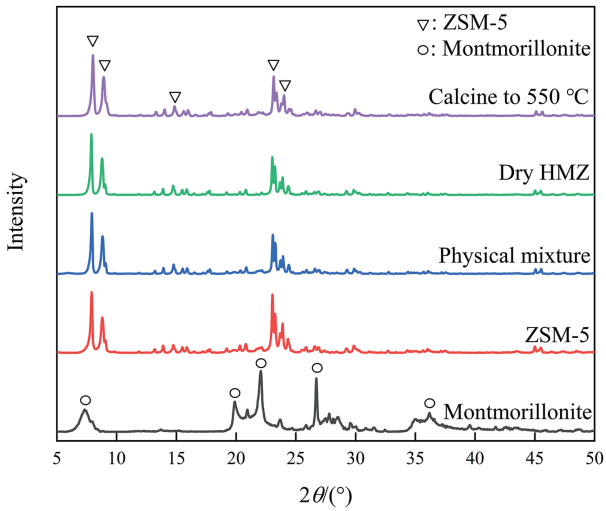


Fig. 12. XRD patterns of raw materials and samples (the physical mixture contains ZSM-5 and montmorillonite in a 4:1 ratio).

water and LAE-9 (30 °C–280 °C, 1.77%), rapid decomposition of cellulose and organic solvents (280 °C–430 °C, 7.42%), and dehydrogenation of montmorillonite (430 °C–600 °C, 1.34%). ZSM-5 powder and powder mixture (ZSM-5:montmorillonite = 4:1) exhibited similar TGA curves. The mass loss of ZSM-5 power was due to the evaporation of water between 30 °C and 150 °C, reaching a plateau at ~450 °C. In contrast, the mass loss of montmorillonite was attributed to the removal of adsorbed water (30 °C–150 °C) and interlayer water (above 150 °C) [25]. Interestingly, despite having the same content of zeolite and clay, the TGA curves of powder mixture and dry HMZs were considerably different due to the absence of organic substances such as cellulose in the powder mixture. In addition, almost no mass loss was observed for the powder mixture, particularly at 430 °C–600 °C, because the liquid water used as a dispersant during HMZ preparation hydrated montmorillonite [26]. Differential scanning calorimetry (DSC) analysis showed that dry HMZs underwent repeated endothermic and exothermic reactions at ~550 °C, suggesting the loss of hydroxyl groups from the montmorillonite structure [27].

The effect of montmorillonite on ZSM-5 during HMZ preparation was investigated *via* XRD. As shown in Fig. 12, physical mixture, dry HMZ and calcined HZM at 550 °C all exhibited distinct ZSM-5 Bragg peaks, indicating that the crystal structures of ZSM-5 remained unchanged before and after extrusion. And the montmorillonite peak in HMZ exhibited a broad background due to its low concentration. Moreover, the ZSM-5 Bragg peak of HZM calcined to 550 °C slightly shifted to higher 2θ, particularly at 7.5°–9.5° and 22.5°–24.5°. High temperatures eliminated the activity of the montmorillonite and destroyed its specific surface area. It may be that a small quantity of ZSM-5 particles was more easily coated by montmorillonite [28,29].

Fig. 13 shows the SEM images of ZSM-5 powder, dry HMZs, and HMZs calcined to 550 °C. ZSM-5 powder consists of particles with a hexagonal plate-like structure (Fig. 13(a)). And ZSM-5 exhibits disordered distribution with high interparticle spacing. After extrusion, the particle spacing of ZSM-5 in HMZs sharply decreased and the particles became more orderly due to the rheological effect of the paste. However, ZSM-5 in dried HMZs had a high tendency to form large clusters due to the introduction of cellulose and montmorillonite (Fig. 13(b)). HMZs calcined at 550 °C primarily contained ZSM-5 particles and clusters, indicating the

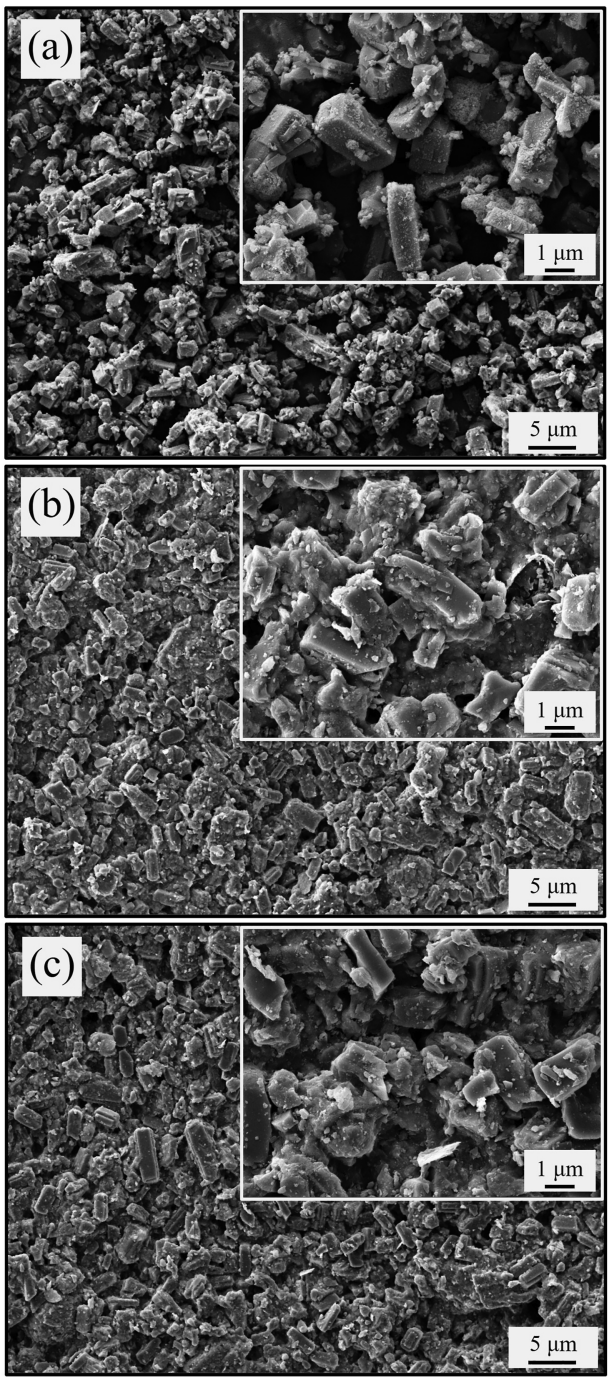


Fig. 13. SEM images: (a) ZSM-5 powder, (b) dry HMZs, (c) HMZs calcined to 550 °C.

uniform distribution of montmorillonite and ZSM-5 within the HMZs (Fig. 13(c)). Interestingly, the crystal morphology of ZSM-5 remained unchanged even after calcination at 550 °C.

To investigate changes in the porosity of ZSM-5 zeolite after vacuum refining and extrusion, argon physical adsorption was applied at 87 K. According to IUPAC classification, the argon adsorption isotherm of ZSM-5 showed type I behavior (Fig. 14(a)). And the smaller hysteresis loop at $P/P_0 > 0.8$ may correspond to the inter-crystalline mesopores and macropores of aggregated small ZSM-5 crystals [30,31]. The uptake of montmorillonite increased under high relative pressure, indicating the presence of meso-

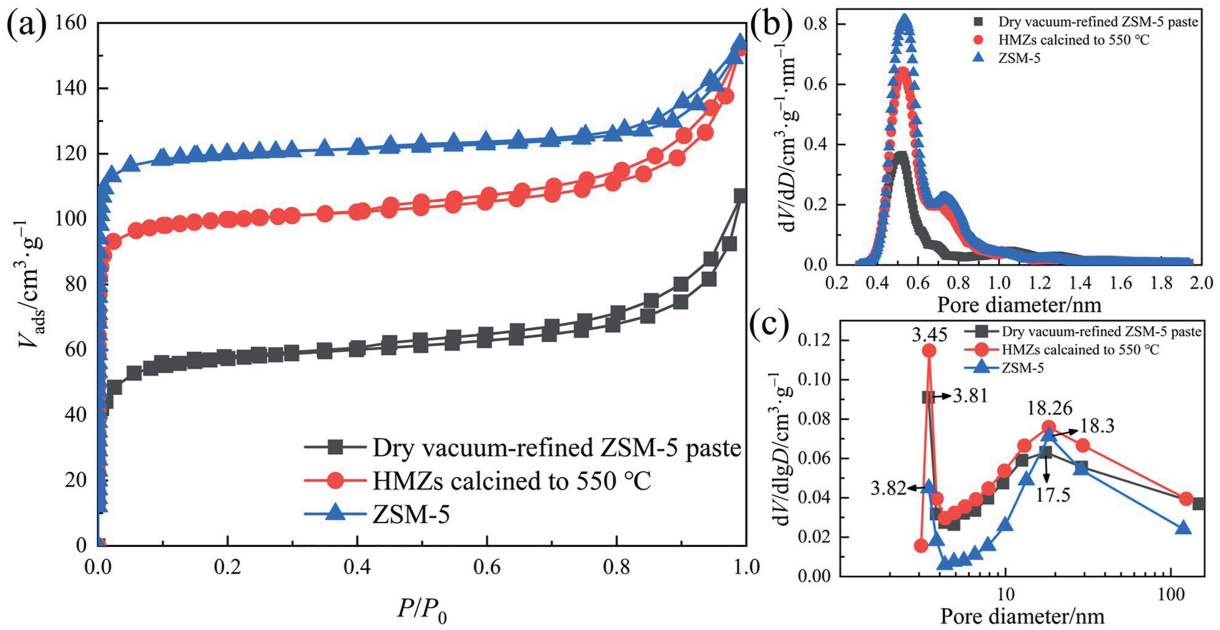


Fig. 14. Argon adsorption–desorption isotherms (a), micropore size distribution (b) and mesopore size distribution curves (c) of dry vacuum-refined ZSM-5 paste, HMZs and ZSM-5.

Table 1
Porous properties of HMZs, ZSM-5 and montmorillonite.

Sample	Surface area/m^2·g^{-1}			Volume/cm^3·g^{-1}		
	BET①	Micropore②	Mesopore③	Total④	Micropore②	Mesopore③
Dry vacuum-refined ZSM-5 paste	220	193.8	23.2	0.163	0.078	0.084
Power mixture (ZSM-5:montmorillonite = 4:1)	400	371.4	27.7	0.262	0.141	0.092
HMZs calcined to 550 °C	400	371.5	26.4	0.261	0.141	0.091
ZSM-5	496	477.7	13.2	0.279	0.181	0.056
Montmorillonite	45	0	44.6	0.173	0	0.173

① BET surface area calculated from the adsorption.
② *t*-plot method.
③ BJH method.
④ Pore volume estimated from the single-point amount adsorbed at $P/P_0 = 0.95$.

macropores and belonging to type II isotherm (Fig. S1). The argon adsorption–desorption isotherms of HMZs resembled those of ZSM-5 and exhibited a larger hysteresis loop. Among them, the hysteresis loop of dry vacuum-refined ZSM-5 paste had a significant reduction due to the incorporation of ZSM-5 and binders (montmorillonite and cellulose), but it could be greatly optimized after calcination. The main peak of micropore size distribution was located at ~0.45 nm (Fig. 14(b)). The mesoporous pore size distribution of ZSM-5 exhibited peaks at 3.82 nm and 18.3 nm (Fig. 14(c)). Interestingly, the dry vacuum-refined ZSM-5 paste displayed a peak at 17.5 nm, indicating that the binders mainly occupied the 18.3 nm pore size of ZSM-5. In contrast, the calcined HMZs revealed a peak at 3.45 nm, suggesting that the calcined montmorillonite mainly occupied the 3.82 nm pores of ZSM-5. The BET surface areas and micropore volumes of power mixture (ZSM-5:montmorillonite = 4:1) and HMZs calcined at 550 °C were almost identical (Table 1). It seemed that the porosity of ZSM-5 in HMZs did not appear to decrease after extrusion and calcination, indicating that there was no significant chemical reaction between montmorillonite and ZSM-5. However, the surface areas and pore volumes of dry vacuum-refined ZSM-5 paste decreased significantly. And it was attributed to the binder blocking the pores of the ZSM-5.

4. Conclusions

In this study, the effects of composition and preparation processes of zeolite pastes on their extrusion behaviors were systematically investigated. A new method for analyzing the plastic deformation behavior of zeolites (elastic zone, yield zone, and plastic zone) was developed based on the stress–deformation curves of ZSM-5 zeolite pastes. In addition, empirical equations for calculating the extrusion workability of ZSM-5 zeolite pastes were derived.

Inorganic binders (kaolin, attapulgite, and montmorillonite) and organic binders (MC, EC, and HPMC) mainly influenced the elastic and plastic zones in the stress–deformation curves, respectively. The ZSM-5 zeolite paste containing montmorillonite and HPMC exhibited superior plasticity. The liquid–solid ratio and LAE-9 content influenced the resistance between zeolite and clay particles. ZSM-5 zeolite pastes with a liquid–solid ratio of 44.5 satisfied the plastic-zone conditions without the influence of deformation rates and exhibited optimized extrusion workability. And an LAE-9 mass content more than 3.2% effectively improved the plasticity of HMZs. Furthermore, vacuum refining considerably enhanced the extrusion workability.

The optimized ZSM-5 zeolite paste exhibited consistent fluidity and stability across various dies and extrusion flow rates, confirming the accuracy of the predicted extrusion workability. In addition, microwave drying followed by calcination at 550 °C effectively preserved the structural integrity of the HMZs. The method proposed in this study can determine the extrusion workability of zeolite-based pastes with high moisture content, and zeolites with different Si/Al ratios and types would be suitable. However, it is not suitable for paste with low moisture content due to its easy cracking during extrusion. In addition, it is necessary to study the extrusion workability of low moisture content pastes in the future.

CRediT Authorship Contribution Statement

Zihao Zhou: Writing – original draft, Methodology, Investigation, Data curation. Yingshu Liu: Supervision, Resources, Funding acquisition. Ningqi Sun: Writing – review & editing, Funding acquisition. Ziyi Li: Writing – review & editing, Funding acquisition, Conceptualization.

Declaration of Competing Interest

The authors declare that they have no known competing financial interests or personal relationships that could have appeared to influence the work reported in this paper.

Acknowledgements

This work was supported by the National Key Research and Development Program of China (2022YFC2403702), the National Natural Science Foundation Program of China (52370107), the Beijing Natural Science Foundation (L233015), Beijing Nova Program (20240484685), and the Fundamental Research Funds for the Central Universities (FRF-EYIT-23-02, FRFIDRYGD21-02).

Supplementary Material

Supplementary data to this article can be found online at https://doi.org/10.1016/j.cjche.2025.12.037.

References

[1] N. Kordala, M. Wyszkowski, Zeolite properties, methods of synthesis, and selected applications, *Molecules* 29 (5) (2024) 1069.
[2] S.Y. Zhang, L. Yao, B. Xu, L. Yang, Z.D. Dai, W.J. Jiang, Recent advances in zeolite-based materials for volatile organic compounds adsorption, *Sep. Purif. Technol.* 350 (2024) 127742.
[3] Q.M. Wu, H.M. Luan, F.S. Xiao, Targeted synthesis of zeolites from calculated interaction between zeolite structure and organic template, *Natl. Sci. Rev.* 9 (9) (2022) nwac023.
[4] B. Bensafi, N. Chouat, F. Djafri, The universal zeolite ZSM-5: structure and synthesis strategies. A review, *Coord. Chem. Rev.* 496 (2023) 215397.
[5] K.Y. Yang, D.Z. Zhang, M.M. Zou, L.L. Yu, S.J. Huang, The known and overlooked sides of zeolite-extrudate catalysts, *ChemCatChem* 13 (6) (2021) 1414–1423.
[6] R. Bingre, B. Louis, P. Nguyen, An overview on zeolite shaping technology and solutions to overcome diffusion limitations, *Catalysts* 8 (4) (2018) 163.
[7] Z. Asgar Pour, M.M. Abduljawad, Y.A. Alassmy, L. Cardon, P.H.M. van Steenberge, K.O. Sebakhy, A comparative review of binder-containing extrusion and alternative shaping techniques for structuring of zeolites into different geometrical bodies, *Catalysts* 13 (4) (2023) 656.
[8] A. Aranzabal, D. Iturbe, M. Romero-Sáez, M.P. González-Marcos, J.R. González-Velasco, J.A. González-Marcos, Optimization of process parameters on the extrusion of honeycomb shaped monolith of H-ZSM-5 zeolite, *Chem. Eng. J.* 162 (1) (2010) 415–423.
[9] P. Guilherme, M.J. Ribeiro, J.A. Labrincha, Behaviour of different industrial ceramic pastes in extrusion process, *Adv. Appl. Ceram.* 108 (6) (2009) 347–351.
[10] F. Raupp-Pereira, M.J. Ribeiro, A.M. Segadães, J.A. Labrincha, Extrusion and property characterisation of waste-based ceramic formulations, *J. Eur. Ceram. Soc.* 27 (5) (2007) 2333–2340.
[11] M.B. Yue, N. Yang, W.Q. Jiao, Y.M. Wang, M.Y. He, Dry-gel synthesis of shaped binderless zeolites composed of nanosized ZSM-5, *Solid State Sci.* 20 (2013) 1–7.
[12] G.E. Barnes, Workability of clay mixtures, *Appl. Clay Sci.* 153 (2018) 107–112.
[13] Y.Y. Li, S.P. Perera, B.D. Crittenden, J. Bridgwater, The effect of the binder on the manufacture of a 5A zeolite monolith, *Powder Technol.* 116 (1) (2001) 85–96.
[14] F.A. Andrade, H.A. Al-Qureshi, D. Hotza, Measuring the plasticity of clays: a review, *Appl. Clay Sci.* 51 (1–2) (2011) 1–7.
[15] B. Baran, T. Ertürk, Y. Sarıkaya, T. Alemdaroğlu, Workability test method for metals applied to examine a workability measure (plastic limit) for clays, *Appl. Clay Sci.* 20 (1–2) (2001) 53–63.
[16] H.A. Tajiri, E.R. de Pieri, H.A. Al-Qureshi, Modified modeling of clay paste extrusion through a circular die: beyond the steady-state, *Int. J. Metall. Met. Phys.* 4 (1) (2019) 27.
[17] H.A. Al-Qureshi, A. Galiotto, A.N. Klein, On the mechanics of cold die compaction for powder metallurgy, *J. Mater. Process. Technol.* 166 (1) (2005) 135–143.
[18] Y.P. Li, E. Onodera, H. Matsumoto, A. Chiba, Correcting the stress-strain curve in hot compression process to high strain level, *Metall. Mater. Trans. A* 40 (4) (2009) 982–990.
[19] M.J. Ribeiro, J.M. Ferreira, J.A. Labrincha, Plastic behaviour of different ceramic pastes processed by extrusion, *Ceram. Int.* 31 (4) (2005) 515–519.
[20] F.A. de Andrade, H.A. Al-Qureshi, D. Hotza, Measuring and modeling the plasticity of clays, *Mater. Res.* 13 (3) (2010) 395–399.
[21] A.A. Brown, D.J. Bammann, Validation of a model for static and dynamic recrystallization in metals, *Int. J. Plast.* 32-33 (2012) 17–35.
[22] K.K. Alaneme, E.A. Okotete, Recrystallization mechanisms and microstructure development in emerging metallic materials: a review, *J. Sci. Adv. Mater. Dev.* 4 (1) (2019) 19–33.
[23] H. Levine, L. Slade, Water as a plasticizer: physico-chemical aspects of low-moisture polymeric systems, in: Water Science Reviews, F. Franks (Ed.), Cambridge University Press, Cambridge, 1988, 79–185.
[24] Z.Y. Li, W. Zhou, Z.H. Zhou, N.Q. Sun, Y.S. Liu, W.H. Liu, X. Yang, D.Y.H. Pui, Microwave drying coupled with convective air and steam for efficient dehydration of extruded zeolite honeycomb monolith, *Ceram. Int.* 50 (21) (2024) 43674–43682.
[25] L. Andrini, R. Moreira Toja, M.R. Gauna, M.S. Conconi, F.G. Requejo, N.M. Rendtorff, Extended and local structural characterization of a natural and 800 °C fired Na-montmorillonite–Patagonian bentonite by XRD and Al/Si XANES, *Appl. Clay Sci.* 137 (2017) 233–240.
[26] S. Karaborni, B. Smit, W. Heidug, J. Urai, E. van Oort, The swelling of clays: molecular simulations of the hydration of montmorillonite, *Science* 271 (5252) (1996) 1102–1104.
[27] F. Ayari, E. Srasra, M. Trabelsi-Ayadi, Characterization of bentonitic clays and their use as adsorbent, *Desalination* 185 (1–3) (2005) 391–397.
[28] R.V. Jasra, B. Tyagi, Y.M. Badheka, V.N. Choudary, T.S.G. Bhat, Effect of clay binder on sorption and catalytic properties of zeolite pellets, *Ind. Eng. Chem. Res.* 42 (14) (2003) 3263–3272.
[29] G.T. Whiting, A.D. Chowdhury, R. Oord, P. Paalanen, B.M. Weckhuysen, The curious case of zeolite–clay/binder interactions and their consequences for catalyst preparation, *Faraday Discuss* 188 (2016) 369–386.
[30] Y.R. Wang, Y. Chang, M. Liu, A.F. Zhang, X.W. Guo, A facile strategy to prepare shaped ZSM-5 catalysts with enhanced para-xylene selectivity and stability for toluene methylation: the effect of *in situ* modification by attapulgite, *Molecules* 24 (19) (2019) 3462.
[31] M. Thommes, K. Kaneko, A.V. Neimark, J.P. Olivier, F. Rodriguez-Reinoso, J. Rouquerol, K.S.W. Sing, Physisorption of gases, with special reference to the evaluation of surface area and pore size distribution (IUPAC technical report), *Pure Appl. Chem.* 87 (9–10) (2015) 1051–1069.